Available online at www.sciencedirect.com
ScienceDirect
Solid State Sciences 10 (2008) 1910–1915
www.elsevier.com/locate/ssscie

Magnetic structure of the inverse perovskite $(Ce_3N)In$

Frank Gäbler [a], Walter Schnelle [b], Anatoliy Senyshyn [c,d], Rainer Niewa [a,*]

[a] Department Chemie, Technische Universität München, Lichtenbergstr. 4, 85747 Garching, Germany
[b] Max-Planck-Institut für Chemische Physik fester Stoffe, Nöthnitzer Str. 40, 01187 Dresden, Germany
[c] Strukturforschung, Materialwissenschaft, Technische Universität Darmstadt, Petersenstr. 23, 64287 Darmstadt, Germany
[d] Forschungsneutronenquelle Heinz Maier-Leibnitz (FRM-II), Technische Universität München, Lichtenbergstr. 1, 85747 Garching, Germany

Received 1 February 2008; received in revised form 11 March 2008; accepted 12 March 2008
Available online 19 March 2008

Abstract

Single-phase microcrystalline powder $(Ce_3N)In$ was prepared by reaction of CeN, Ce and In. The magnetic moments located on the cerium atoms in the inverse cubic perovskite (space group $Pm\bar{3}m$, $Z = 1$, $a = 5.0416(4)$ Å) order antiferromagnetically below 9(1) K. Application of an external magnetic field reveals a multistep metamagnetic behavior. Neutron diffraction was performed at various temperatures without application of external magnetic fields. Below T_N additional reflections due to magnetic order correspond to a magnetic propagation vector of $\boldsymbol{k} = (0, ½, ½)$. Refinements of the magnetic structure well below T_N lead to three independent magnetic substructures parallel to the crystallographic axes. All three magnetic substructures are internally antiferromagnetically ordered resulting in a zero net magnetic moment.

Keywords: Nitride; Magnetic structure; Cerium; Indium; Neutron powder diffraction

1. Introduction

Metal-rich perovskites with general composition $(M_3Z)M'$ (M = metal, Z = electronegative element, mostly C, N, O) were obtained with a multitude of different element combinations within recent years. The nitrides of different 3d-metals, mostly with iron as majority component, and the general composition $(Fe_3N)M$ have attracted particular attention due to their electronic properties [1–4]. Most of the characterized phases crystallize with the cubic perovskite structure, however, distortion variants to orthorhombic perovskites, several stacking variants of hexagonal perovskites as well as a related Ruddlesden–Popper series are known for the respective metal-rich ternary alkaline-earth metal nitrides $(A_3N_x)E$ (A = alkaline-earth metal, E = p-group element of the third or higher period, and x typically close to 1) [5–7]. From the extremely broad range of different metal-rich perovskite systems, particular compounds with alkaline-earth metals as majority component cover semiconductors (involving exclusively closed shell ions) as well as electron-deficient metals according to a simple electron counting [7–12]. Replacement of the divalent alkaline-earth metal species by trivalent rare-earth metals inverts the electronic balance to electron-rich systems leading intrinsically to metals. Additionally, it gives the possibility to introduce localized magnetic moments [13–16].

The resulting magnetic properties of the rare-earth metal nitrides $(R_3N_x)E$, where R is a rare-earth metal element, depend on the kind of rare-earth metal, its electronic configuration, the distance between the rare-earth metal species, and the electronic balance within the compound. Obviously, the latter two parameters can be easily tuned by the nature of the component E (main-group element, e.g. Al, Ga, In, Sn).

In the present work we analyze the magnetic properties of $(Ce_3N)In$ and determine the magnetic spin structure in the antiferromagnetic state. The term metamagnetism, in this context, will be used for any type of field-induced magnetic transition, in particular for processes breaking antiferromagnetic spin structures, typically leading to spin structures with higher magnetic moments and finally to a saturated ferromagnetic spin structure [17,18].

* Corresponding author. Tel.: +49 89 289 13111; fax: +49 89 289 13762.
E-mail address: rainer.niewa@mytum.de (R. Niewa).

1293-2558/$ - see front matter © 2008 Elsevier Masson SAS. All rights reserved.
doi:10.1016/j.solidstatesciences.2008.03.010

2. Experimental

2.1. Synthesis

Since rare-earth metals and all products in this study are air and moisture sensitive, all manipulations were carried out under inert conditions in an argon filled glove box (MBraun, O_2 and H_2O content <1 ppm).

$(Ce_3N)In$ was prepared by reaction of CeN, Ce and In, where for the preparation of CeN metallic Ce (Hunan Institute of Rare Earth Materials, 99.9% metal based; additionally purified by a remelting procedure) was heated in a Ta-crucible under static nitrogen atmosphere (Messer–Griesheim, 99.999%, additionally purified by passing over molsieve, Roth 3 Å, and BTS-catalyst, Merck) in a high-frequency-furnace (TIG 5/300, Hüttinger) to temperatures up to about 1400 K. The reaction was completed in a tube-furnace at 1120 K under nitrogen of ambient back-pressure.

Further on, the respective molar ratios of CeN, Ce and In (99.9999% Chempur) were fused in an arc-furnace. The resulting melt-bead was wrapped in molybdenum foil and sealed in an evacuated fused silica ampoule. This assembly was annealed at 1220 K for seven days. In a previous publication a single-phase $(Ce_3N)In$ sample with composition $(Ce_3N_{0.92(1)})In$ according to neutron and X-ray powder diffraction and chemical analyses was characterized in-depth [14].

2.2. Characterization

2.2.1. X-ray diffraction

For X-ray diffraction the powdered samples were loaded between two Kapton-foils for protection from moisture and air. The X-ray experiments were carried out on an imaging plate Guinier-camera (Huber-Diffraction, G 670) equipped with a quartz monochromator (Cu Kα_1-radiation, $6° \leq \Theta \leq 100°$, 4×15 min). According to the resulting pattern, single-phase material $(Ce_3N)In$ was obtained.

2.2.2. Neutron diffraction

Neutron diffraction experiments were carried out on the powder diffractometers E6 and E9 at BENSC, Hahn–Meitner-Institut (Berlin, Germany) and SPODI at FRM-II (Garching, Germany) [19]. The powdered sample was loaded under argon in a cylindrical vanadium container (diameter 6 mm for E6 and E9, 8 mm for SPODI; length 51 mm; wall thickness 0.15 mm) and sealed with an indium gasket. Diffraction patterns were collected at 1.8 K (E6); 1.8 K, 298 K (E9); 3.4 K, 6 K, 8 K, 10 K, 15 K, and 300 K (SPODI).

Rietveld refinements were carried out using the software package FullProf [20,21]. Pseudo-Voigt function was chosen to model the peak profile shape of E6 and SPODI instruments, whereas for simulation of E9 data the modified Thompson–Cox–Hastings pseudo-Voigt function was applied. The background contribution has been determined using a linear interpolation between selected data points in non-overlapping regions. The scale factor, zero angular shift, profile shape parameters (for E6 and SPODI data), half width parameters, asymmetry (for E6 and SPODI data) and lattice parameters as well as atomic displacement parameters were varied during the fitting. A cylindrical absorption correction has been applied for all datasets, where the product of the linear absorption coefficient and the cylinder radius μR was equal to 0.3165, 0.2325 and 0.3204 for E6, E9 and SPODI data, respectively. Finally, the occupancy parameters were also varied.

Unfortunately, no experimental magnetic Ce^{3+} form factors have been found in the literature. As an alternative, a theoretical value of the magnetic form factor has been used [22]. Obtained coefficients in Brown's notation (A, a, B, b, C, c, D) [23] are represented by the following values: −0.409(7), 5.90(5), −0.580(6), 1.94(2), 0, 0, −0.0119(8). Best results of Rietveld refinement fits were obtained with the parameters listed in Table 1.

2.2.3. Magnetization measurements

Measurements of the magnetic susceptibilities were carried out on a SQUID magnetometer (MPMS-XL7, Quantum

Table 1
Experimental structural parameters of $(Ce_3In)N$ at various temperatures (space group $Pm\bar{3}m$)

Sample no.	Sample 1			Sample 2					
Instrument used	E6	E9		SPODI					
Wavelength λ, Å	2.452	1.798		1.548					
Temperature, K	1.8	1.8	298	3.4	6	8	10	15	300
Cell size a, Å	5.0289(8)	5.04464(7)	5.05046(9)	5.03823(8)	5.03818(8)	5.03819(8)	5.0391(3)	5.0392(3)	5.0476(4)
B_{iso} (Ce), Å^2	0.9(4)[a]	0.16(7)	0.50(8)	0.11(2)	0.11(2)	0.14(2)	0.12(2)	0.13(2)	0.75(2)
B_{iso} (In), Å^2	0.9(4)[a]	0.3(1)	0.5(1)	0.00(3)	0.02(3)	0.04(2)	0.08(3)	0.03(3)	0.71(3)
B_{iso} (N), Å^2	0.9(4)[a]	0.39(7)	0.34(7)	0.24(2)	0.27(2)	0.21(2)	0.26(2)	0.24(2)	0.64(2)
N site occupation, %	89.4(8)	95(1)	92(2)	91.3(5)	92.1(5)	90.7(4)	91.6(5)	91.3(5)	92.0(5)
μ(Ce), μ_B	1.83(3)	1.75(8)	–	1.28(2)	1.22(3)	0.68(3)	–	–	–
Quality of fit:									
R_p, %	3.50	4.11	4.13	3.27	3.36	3.20	3.22	3.25	3.02
R_{wp}, %	4.58	5.32	5.50	3.96	4.03	4.02	4.00	4.07	3.71
R_{exp}, %	1.85	3.49	3.39	5.72	5.68	5.80	5.76	5.75	5.79

The structural data were modeled with Ce occupying the 3c site (1/2, 1/2, 0), In in 1a (0, 0, 0) and N in 1b (1/2, 1/2, 1/2). Numbers in parentheses give statistical inaccuracies in the last significant digit.

[a] Because of observed correlations an overall B has been refined instead of B_{iso}.

Design) at fields $\mu_0 H$ between 2 mT and 7 T in the 1.8–400 K range, using about 100 mg of single-phase material sealed in a quartz-tube under 400 mbar He.

3. Results and discussion

Only Bragg reflections belonging to compound with $Pm\bar{3}m$ symmetry were observed in X-ray diffraction pattern for sample 1 $(Ce_3N)In$ [14], whereas neutron powder diffraction has deduced weak (ca. 0.3% w/w) traces of CeN. Therefore, an additional attempt to synthesize phase pure $(Ce_3N)In$ was made (sample 2). Both X-ray and neutron powder diffractions reveal the single-phase composition. The magnetic behavior and electric behavior of the newly prepared sample (sample 2) and the previously reported sample are nearly identical, although the composition differs slightly in nitrogen content obtained by structure Rietveld refinement. The cubic unit cell at ambient temperature for the new sample from X-ray powder diffraction resulted in $a = 5.0416(4)$ Å compared to 5.0489(2) Å for $(Ce_3N_{0.92(1)})In$ from our previous study [14].

3.1. Nuclear crystal structure

The diffraction data clearly are compatible with the motif of an inverse cubic perovskite, i.e., nitride ions octahedrally surrounded by cerium species and indium atoms in the large cuboctahedral voids (Fig. 1). No indications for a distortion from cubic metric were observed in any diffraction pattern. The structure refinements indicate a significant nitrogen deficiency $(Ce_3N_{0.92(1)})In$, as was previously observed for a similar sample $(Ce_3N_{0.92(1)})In$ (according to X-ray and neutron powder diffractions and chemical analyses) [14]. No indications for an ordered arrangement of the vacancies were apparent from diffraction data.

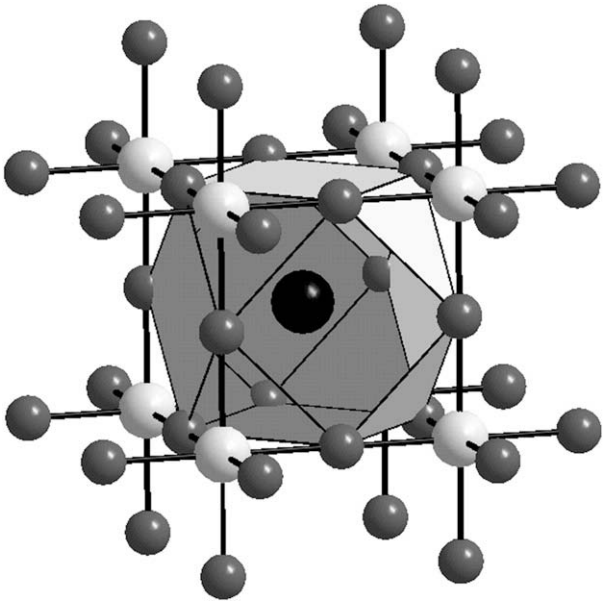

Fig. 1. Nuclear structure of $(Ce_3N)In$, N: light grey spheres, Ce: smaller dark grey spheres, In: black sphere.

3.2. Magnetic properties

The magnetic properties of the metallic $(Ce_3N)In$ are dominated by the magnetic moment of Ce. Above 100 K $(Ce_3N)In$ displays a behavior which can be approximated by Curie–Weiss law (see Fig. 2), however, at lower T deviations are evident due to the crystal field splitting of the ground state multiplet. For $(Ce_3N)In$ a fit of Curie–Weiss law for $100\ \mathrm{K} < T < 400\ \mathrm{K}$ yields an effective magnetic moment μ_{eff}/Ce-atom $= 2.44\ \mu_B$ ($\theta = -17(1)$ K). From a low-temperature Curie–Weiss fit (for $20\ \mathrm{K} < T < 100\ \mathrm{K}$) a more reliable $\theta_{\mathrm{LT}} = -5.4(1)$ K is deduced. The curve of $n_{\mathrm{eff}}(T)$ is consistent with the $^2F_{5/2}$ ground state of Ce^{3+} ($4f^1$) [24]. X-ray absorption spectroscopy additionally confirmed that there is no significant admixture of the $4f^0$ state of Ce [14]. At low temperatures the magnetic moments localized on the cerium atoms in $(Ce_3N)In$ order antiferromagnetically, as is indicated by a cusp in $\chi(T)$ at $T_N = 9.0(2)$ K (Fig. 2). We already notice an unusual broad signal in the susceptibility due to the antiferromagnetic order.

The isothermal magnetization measurements show metamagnetic behavior of $(Ce_3N)In$ with several steps in magnetization curve. Fig. 3 displays the magnetization per formula

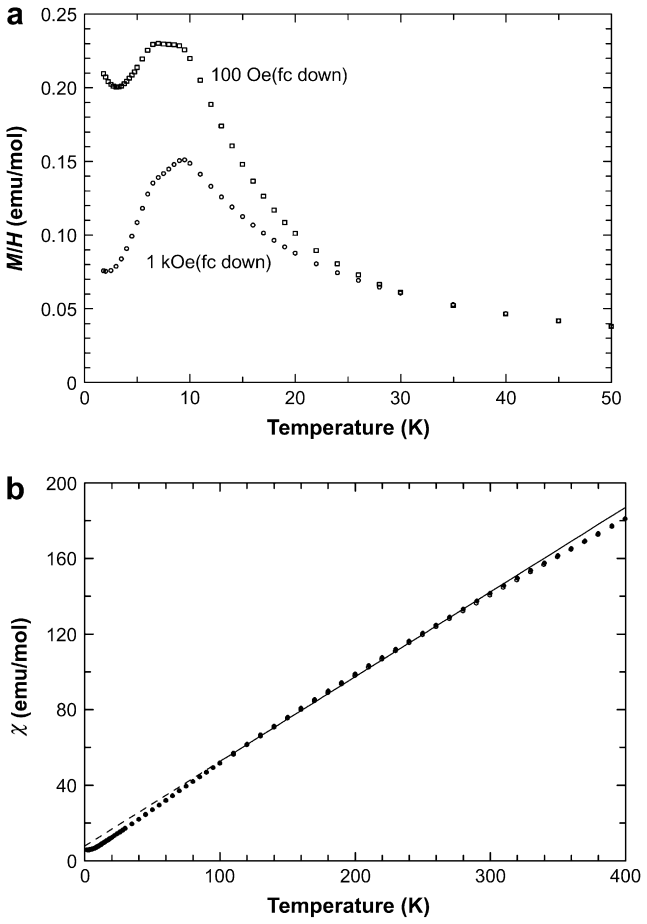

Fig. 2. (a) Magnetization of $(Ce_3N)In$ measured in different external magnetic fields showing the antiferromagnetic transition at $T_N = 9.0$ K, (b) magnetic susceptibility of $(Ce_3N)In$ and fitting of the data above $T = 100$ K to Curie–Weiss law (straight line).

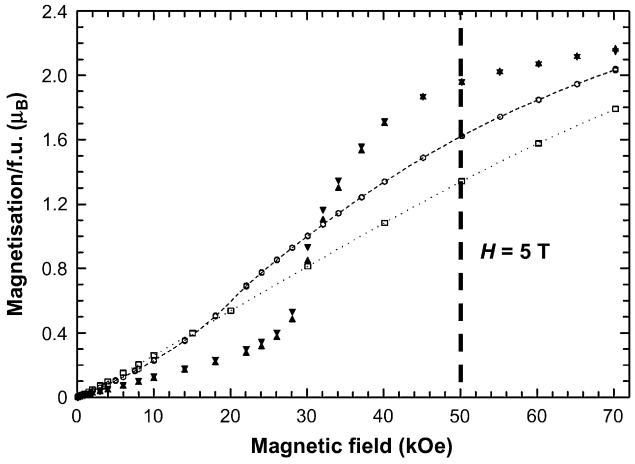

Fig. 3. Magnetization per formula unit of $(Ce_3N)In$ as a function of the external magnetic field at different temperatures (triangles: $T = 2.0$ K, circles: $T = 5.0$ K, squares: $T = 8.0$ K, the orientation of the triangle symbols indicates the field sweep directions).

unit *versus* external magnetic field for different temperatures. At a temperature of 2 K, which is sufficiently below the Néel temperature, the step size can be approximately quantified. The step size of the first well-shaped step may represent 1/3 ($g_J J/3 = 2.14\ \mu_B$) of the expected saturated magnetic moment $\mu_{sat} = g_J J = 3 \times 15/7\ \mu_B = 6.43\ \mu_B$. Hence, assuming further steps of equal height, the full development proceeding with increasing magnetic field might be explained by only three steps until saturation is achieved. Similar step-like metamagnetic behavior was also observed for related compounds $(R_3N)E$ (E = Al, Ga, In), e.g., with R = Pr: at 1.8 K three steps of equal height are resolved up to 14 T. For these Pr compounds the step size relative to the expected saturation magnetization, however, is as small as about 1/9 [25]. At $T = 2$ K the transitions observed in $(Ce_3N)In$ show an S-shape appearance, while at $T = 8$ K the transitions are almost wiped out by thermal disorder, as expected from the temperature near $T_N \sim 9$ K at $H_{ext} = 0$.

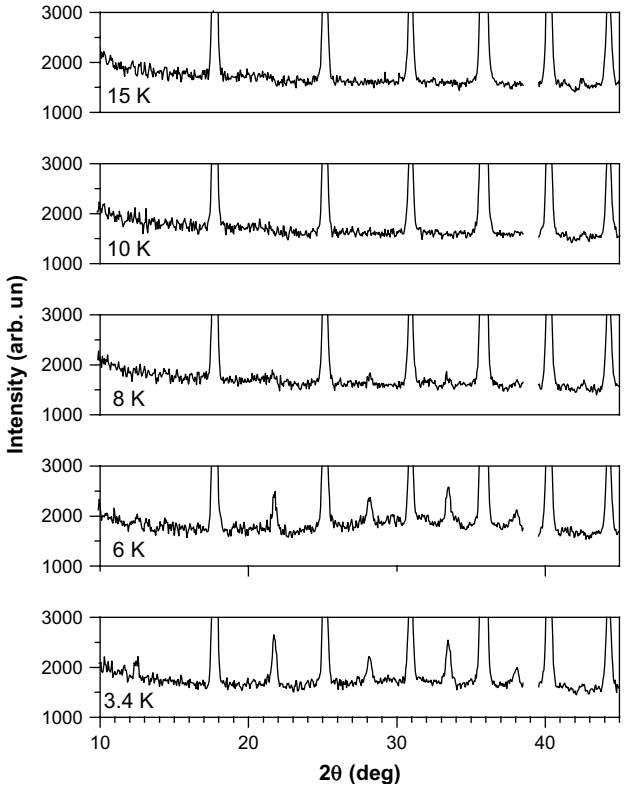

Fig. 4. Evolution of neutron diffraction patterns of $(Ce_3N)In$ ($\lambda = 1.548$ Å) at various temperatures. The gap in the diffraction patterns corresponds to Bragg reflection originating from the walls of the closed-cycle refrigerator.

3.3. Magnetic structure

To analyze the spin structure, neutron powder diffraction at different temperatures (1.8 K, 3 K (well below T_N), 6 K, 8 K, 10 K, 15 K, and 300 K) in the absence of an external magnetic field was performed. The neutron diffraction experiments carried out on $(Ce_3N)In$ at temperatures below $T_N = 9$ K show that additional strong reflections appear, which can be explained by a spin structure with a Néel-type antiferromagnetic ordering (Fig. 4). The magnetic propagation vector was determined to be $\boldsymbol{k}_{mag} = (0, ½, ½)$, i.e., a doubling of the cubic translation metric in two directions for the crystallographic description of the magnetic structure. This propagation vector together with the known nuclear structure serves as an input for further symmetry analysis of possible schemes of magnetic ordering. The representation analysis has been carried out with the program Basireps and all (10) predicted symmetry-allowed spin configurations were checked with Rietveld refinement.

The best fit of magnetic reflections was obtained with the model where orientation of magnetic moments on the Ce^{3+} ($4f^1$) species can be rationalized by three magnetic

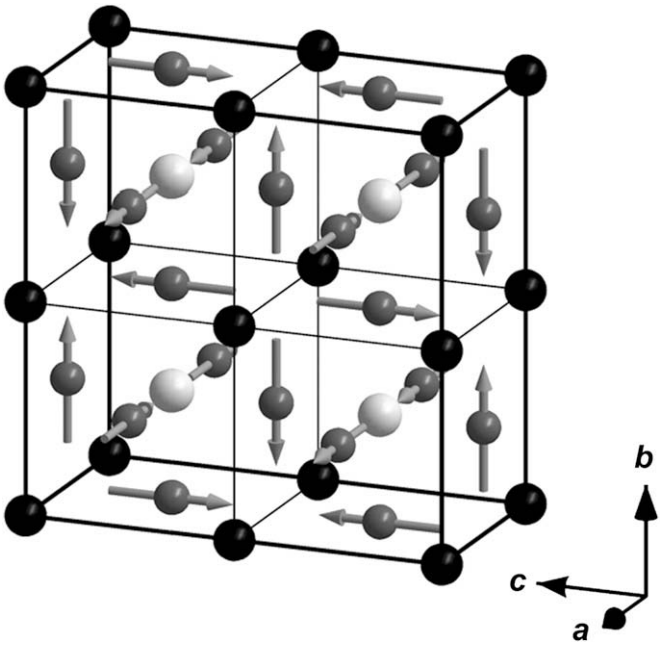

Fig. 5. Zero-field magnetic structure of $(Ce_3N)In$ at 1.8 K. N: light grey spheres, In: black spheres, Ce: grey spheres carrying an arrow indicating the direction of the vector of the magnetic moment. All magnetic vectors are oriented parallel to one crystallographic axis.

substructures with components parallel to the orthogonal crystallographic axes. Each substructure itself is antiferromagnetically ordered and, thus, the magnetic moments cancel. All magnetic components of the substructures are oriented parallel to the crystallographic axes. Those moments parallel to [010] and [001] lead to the necessary doubling of the nuclear unit cell for the description of the magnetic structure. The third magnetic substructure has ferromagnetic contributions within the [100] direction, but neighboring piles are ordered antiferromagnetically. As a result of the proposed magnetic structure all nitrogen species are surrounded equally by six Ce^{3+} ($4f^1$) species every two of which belong to one of the three substructures. The magnetic symmetry has been found consistent with the $P2m'm'$ space group, arising from $Pm\bar{3}m$ via $Pmm'm'$ supergroup. Fig. 5 suggests a magnetic structure for the antiferromagnetic state of $(Ce_3N)In$ based on the refinement of the pattern taken at 3 K (refinement depicted in Fig. 6).

The magnetic moment at Ce for the lowest temperature of 1.8 K refines to 1.75(8) μ_B (the free saturation moment of Ce^{3+} ($4f^1$) is 2.143 μ_B, for comparison). At elevated temperatures approaching $T_{Néel}$ the refined magnetic moment drops significantly to 1.28(2) μ_B at 3 K, 1.22(3) μ_B at 6 K and 0.68(3) μ_B at 8 K indicating an increasing contribution from thermally induced disorder even below $T_{Néel}$. Concomitantly, a quite significant increased background at low temperatures indicates the diffraction intensity owing to short range magnetic ordering (Fig. 4).

4. Summary

Both room-temperature X-ray and neutron powder diffraction experiments confirm that single-phase $(Ce_3N)In$ was obtained from the reaction of CeN, Ce and In. Magnetic susceptibility measurements together with low-temperature neutron diffraction measurements have shown that the magnetic moments located on the cerium atoms in $(Ce_3N)In$ order below $T_{Néel} = 9$ K with a commensurable magnetic structure. The magnetic ordering can be presented as three antiferromagnetic

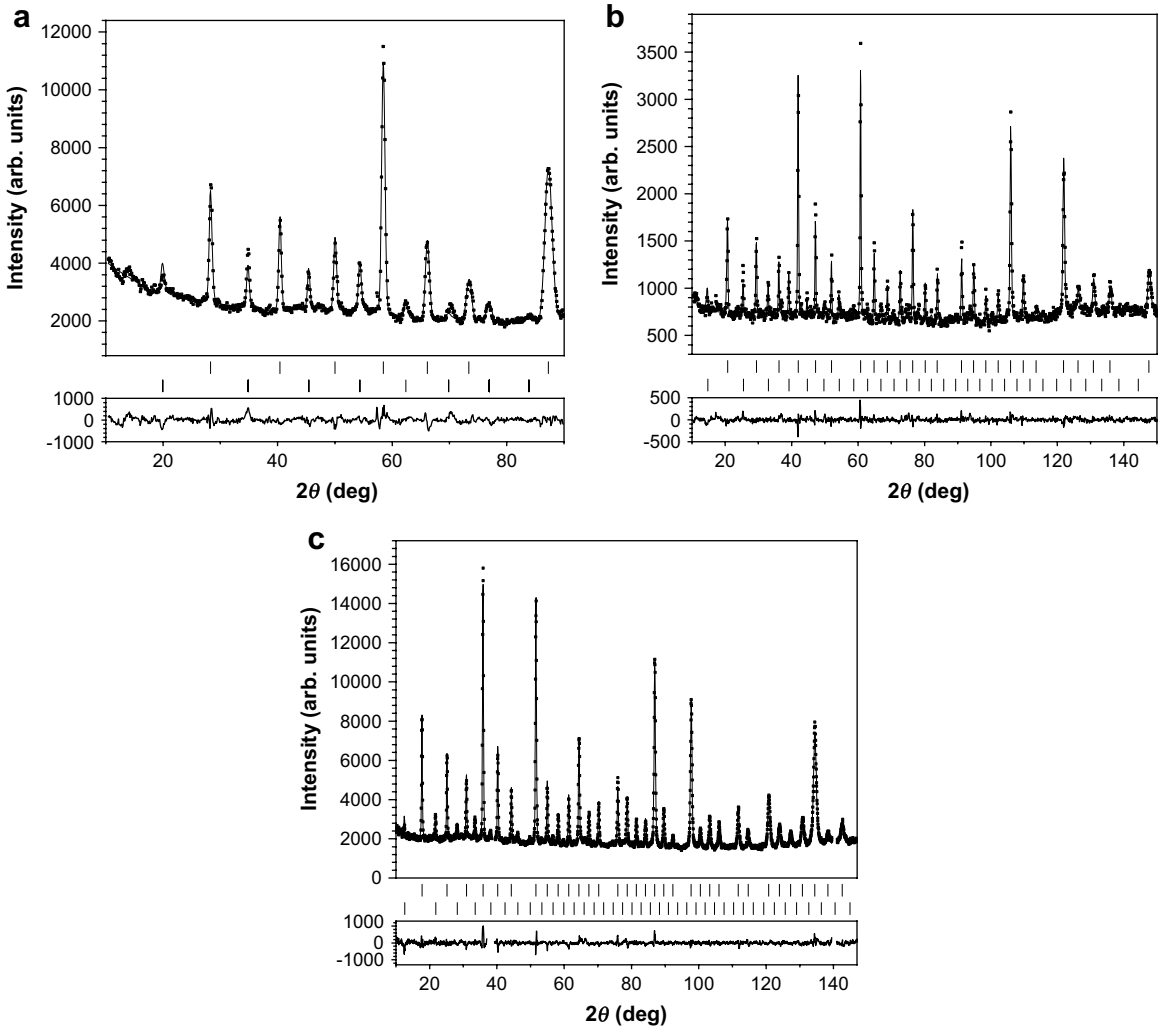

Fig. 6. Result of Rietveld refinements (experimental and calculated profiles together with difference curve) of $(Ce_3N)In$. (a) Diffraction pattern collected at E6 powder diffractometer ($T = 1.8$ K, $\lambda = 2.452$ Å); (b) diffraction pattern collected at E9 powder diffractometer ($T = 1.8$ K, $\lambda = 1.798$ Å); (c) diffraction pattern collected at SPODI powder diffractometer ($T = 3.4$ K, $\lambda = 1.548$ Å). Each upper line of tick marks corresponds to nuclear contributions from $(Ce_3N)In$, the second lines to magnetic contributions. The narrow excluded regions are due to contributions stemming from the cryostat.

substructures with magnetic components parallel to the orthogonal crystallographic axes.

The significant drop of Ce^{3+} magnetic moment (1.75(8) μ_B at 1.8 K; 1.28(2) μ_B at 3 K) might hint to the presence of a commensurate–incommensurate transformation in between those temperatures. However, no direct evidence for such a transition was obvious in high-resolution neutron powder diffraction patterns.

High-field magnetic susceptibility measurements reveal a multistep metamagnetic behavior. Investigations of the magnetic structure of $(Ce_3N)In$ at the first metamagnetic step under high magnetic field are currently underway.

Acknowledgement

This work was supported by the Elitenetzwerk Bayern within the Advanced Materials Science program and by the Deutsche Forschungsgemeinschaft within the priority program 1166 ''Lanthanoidspezifische Funktionalitäten in Molekül und Material''.

References

[1] A. Houben, P. Müller, J. von Appen, H. Lueken, R. Niewa, R. Dronskowski, Angew. Chem., Int. Ed. 44 (2005) 7212.
[2] C.A. Kuhnen, A.V. dos Santos, J. Alloys Compd. 384 (2004) 80.
[3] A.V. dos Santos, C.A. Kuhnen, J. Alloys Compd. 321 (2001) 60.
[4] R.S. de Figueiredo, J. Foct, A.V. dos Santos, C.A. Kuhnen, J. Alloys Compd. 315 (2001) 42.
[5] F. Gäbler, Yu. Prots, R. Niewa, Z. Anorg. Allg. Chem. 633 (2007) 93.
[6] F. Gäbler, R. Niewa, Inorg. Chem. 46 (2007) 859.
[7] M.Y. Chern, D.A. Vennos, F.J. DiSalvo, J. Solid State Chem. 96 (1992) 415.
[8] R. Niewa, W. Schnelle, F.R. Wagner, Z. Anorg. Allg. Chem. 627 (2001) 365.
[9] M.Y. Chern, F.J. DiSalvo, J.B. Parise, J.A. Goldstone, J. Solid State Chem. 96 (1992) 426.
[10] E.O. Chi, W.S. Kim, N.H. Hur, D. Jung, Solid State Commun. 121 (2002) 309.
[11] F. Gäbler, M. Kirchner, W. Schnelle, M. Schmitt, H. Rosner, R. Niewa, Z. Anorg. Allg. Chem. 631 (2005) 397.
[12] F. Gäbler, M. Kirchner, W. Schnelle, U. Schwarz, M. Schmitt, H. Rosner, R. Niewa, Z. Anorg. Allg. Chem. 630 (2004) 2292.
[13] M. Kirchner, F. Gäbler, W. Schnelle, F.R. Wagner, R. Niewa, Z. Kristallogr. 221 (2006) 543.
[14] M. Kirchner, W. Schnelle, F.R. Wagner, R. Niewa, Solid State Sci. 5 (2003) 1247.
[15] M. Kirchner, W. Schnelle, R. Niewa, Z. Anorg. Allg. Chem. 632 (2006) 559.
[16] M. Kirchner, W. Schnelle, R. Niewa, Z. Naturforsch. 61b (2006) 813.
[17] M. Date, J. Magn. Magn. Mater. 90 (1990) 1.
[18] D. Gignoux, D. Schmitt, J. Magn. Magn. Mater. 100 (1991) 99.
[19] M. Hoelzel, A. Senyshyn, R. Gilles, H. Boysen, H. Fuess, Neutron News 18 (2007) 23.
[20] J. Rodriguez-Carvajal, Physica B 192 (1993) 55.
[21] J. Rodríguez-Carvajal, Commission on Powder Diffraction (IUCr) Newsletter 26 (2001) 12.
[22] C. Stassis, H.W. Deckman, B.N. Harmon, J.P. Desclaux, A.J. Freeman, Phys. Rev. B 15 (1977) 369.
[23] P.J. Brown, in: A.J.C. Wilson (Ed.), Magnetic Form Factors, International Tables for Crystallography, vol. C, Kluwer Academic, Dordrecht, 1992, p. 391.
[24] C.S. Garde, J. Ray, J. Magn. Magn. Mater. 189 (1998) 293.
[25] Niewa R., Habilitation Thesis, Universität Dresden, 2005.